



Structural, Morphological, Electrical and Impedance Spectroscopy Investigation of $\text{Pb}_{1/2}\text{Ba}_{1/2}\text{Ni}_{1/2}\text{W}_{1/2}\text{O}_3$ Electronic Material

S. Kalingani¹ · Satyaprakash Narayan Das¹ · S. K. Pradhan¹ · S. Bhuyan¹ · R. N. P. Choudhary¹

Received: 18 February 2022 / Revised: 4 July 2022 / Accepted: 15 July 2022 / Published online: 13 August 2022
© The Korean Institute of Electrical and Electronic Material Engineers 2022

Abstract

In this present study the $(\text{Pb}_{1/2}\text{Ba}_{1/2})(\text{Ni}_{1/2}\text{W}_{1/2})\text{O}_3$, [PBNW] perovskite compound has been formulated and synthesized by adopting a solid-state reaction technique. The detailed structural, morphological, and electrical characterization has been carried out to explore its characteristics for further application in the field of electronic devices and sensors. With the help of x-ray diffraction analysis orthorhombic structure has been recognized. Dielectric, impedance spectroscopy, and a.c. conductivity analysis has been carried out through a wide range of temperatures as well as frequency (temperature range 25–500 °C, frequency range 1 kHz to 1 MHz). Presence of a single semi-circular arc from Nyquist analysis points toward the grain contribution of the sample. An equivalent circuit model has been developed to explore its electrical behavior. The activation energy, as well as the charge carrier mobility, has been estimated. Methodical studies for dielectric properties at high temperatures are accomplished for analysing electrical inhomogeneity allied with surfaces, grain boundaries, or grains, which are imperative for fundamental characterization and device fabrication.

Keywords Perovskite · Dielectric · Impedance spectroscopy · Conductivity

1 Introduction

The perovskite is one of the promising and extraordinary ferroelectric materials in the field of basic as well as applied research. The importance of these materials has been epitomized in various solid-state technologies starting from metallic, superconducting, semiconducting, and insulating properties. These have a vast variety of applications such as capacitors, electronics, solar devices, and electrical devices [1–3], different types of sensors and transducers [4, 5], resonators, phase shifters, filters, oscillators, etc. [6, 7]. The usual form of perovskite structure is given by ABO_3 where mono or divalent atoms are represented by ‘A’ and tri or hexavalent ions are represented by ‘B’. The perovskites can form a wide variety of compounds where A is the alkaline metals and B is the transition elements. Due to the multiple oxidation states of the transition metals, they can have a wide variety of dynamic properties for various applications.

Additionally, any deviance from the usual stoichiometry with the incorporation of ions into the A- and/or B-sites can able to transform the electronic properties of the modified perovskites. Again it is worthy to note that majority of the elements within the periodic table can form a stable perovskite arrangement which gives rise the viability to partial substitution of cations in both the available sites A and B resulting in a general form of $\text{A}_{(1-x)}\text{A}'_x\text{B}_{(1-y)}\text{B}'_y\text{O}_3$. Effect of partial substitution of single site (Either A or B) has been studied such as $\text{AgNb}_{1/2}\text{Ta}_{1/2}\text{O}_3$ [8], $\text{Ca}_{1-x}\text{Sm}_{2x/3}\text{TiO}_3$ [9], $\text{Bi}_{1-x}\text{Nd}_x\text{FeO}_3$ [10], $\text{Ba}(\text{Fe}_{1/3}\text{Nb}_{1/3}\text{Ta}_{1/3})\text{O}_3$ [11], $\text{La}_{1-x}\text{Ce}_x\text{CoO}_3$ [12], $(\text{La}_{0.3}\text{Sr}_{0.7})(\text{Al}_{0.65}\text{Ta}_{0.35})\text{O}_3$ [13], $(\text{La}_{1-x}\text{Sr}_x)(\text{Cr}_{1-y}\text{Fe}_y)\text{O}_{3-\delta}$ and $(\text{La}_{1-x}\text{Sr}_x)(\text{Cr}_{1-y}\text{Ru}_y)\text{O}_{3-\delta}$ [14] etc. Still, research has been going on in this thrust area for the development of new partially substituted perovskites. Joseph et al. [15] also give various catalytic applications of double perovskites. However, there is still no or little consensus in the literature for the composition $\text{A}_{1/2}\text{A}'_{1/2}\text{B}_{1/2}\text{B}'_{1/2}\text{O}_3$ where both the cations are half substituted. Hence an attempt has been made to replace A site with $\text{A}_{1/2}$ and $\text{A}'_{1/2}$ whereas B by $\text{B}_{1/2}$ and $\text{B}'_{1/2}$. In our modified partially substituted complex perovskite structure B and B’ are the transition metals (tungsten and nickel respectively) having relatively less ionic radii, while A is the alkaline earth metal (barium)

✉ Satyaprakash Narayan Das
satyaprakashdas@soa.ac.in

¹ Department of Electronics and Communication Engineering, ITER, Siksha ‘O’ Anusandhan Deemed to be University, Bhubaneswar 751030, India

and A' is the basic metal (Lead) with relatively larger ionic radii has been chosen to satisfy the structural and charge balance neutrality of the chosen perovskites. Here in the compound, $(\text{Pb}_{1/2}\text{Ba}_{1/2})(\text{Ni}_{1/2}\text{W}_{1/2})\text{O}_3$, [PBNW], Ba and Pb are assumed to be located at the body center, atoms Ni and W are assumed to be located at the corner position of the cube, whereas oxygen atoms take the face-centered positions. Given this, here we have synthesized PBNW by the solid-state reaction route and its structural, morphological, dielectric as well as its conductivity property has been explored and communicated through this article.

2 Material Formulation and Its Preparation Method

The PBNW perovskite electro-ceramic solid solution has been synthesized through a high-temperature solid-state reaction technique [16]. The required reagent grade oxide powder of PbO, NiO, WO_3 (obtained from Loba Chemical, India, >99.0% purity) and BaCO_3 (obtained from Sigma-Aldrich, USA, >99.0% purity) are batched in their required stoichiometric ratios. These oxide powders are mixed by using an agate mortar in the atmospheric medium for 1 h to obtain a homogeneous mixture. Further for increasing the homogeneity of the mixture, it is again ground in a liquid medium (presence of acetone) till it gets evaporated. Afterward, the mixture is fired at a temperature of 850 °C (a particular temperature is acquired in a stepwise manner) for 6 h using a microcontroller controlled high-temperature furnace for calcination followed by milling of the lump into powder form again. This calcined powder is used for structural and its lattice parameter analysis by using an x-ray diffractometer (Model: Rigaku, Miniflex, Japan) with a scanning speed of 2°/min, x-ray wavelength (λ) of 1.54 Å, and Bragg angle (θ) ranging from $(20^\circ \leq 2\theta \leq 70^\circ)$. POWD, an interactive software package has been used for refinement of the lattice parameter obtained from all the major reflection peaks of the XRD diffraction data. Based on the good agreement of the measured data and calculated parameters along with the lowest standard deviation, the appropriate crystal system is chosen. The alteration of the lattice parameters of the chosen unit cell can be accepted by using a least-squares sub-routine procedure through the interactive software package. Finally, these powders are mixed with a synthetic binder (PVA, polyvinyl alcohol) for increasing the strength as well as granulation purpose and then the synthesized powders are pressed into required disc-shaped pellet (~10 mm in diameter, 1–2 mm thickness, and 40 MPa pressure) by using a uniaxial circular die punch. These developed pellets are then sintered at a temperature of 900 °C for densification purpose for 6 h in air by progressively increasing the temperature to avoid the development of cracks during the PVA evaporation

process. Then the obtained dense pellet is used for SEM (scanning electron microscopy) micrographs along with EDX (energy dispersive x-ray) analysis purpose which gives a brief idea about the surface morphology and content of different elements respectively. The two surfaces of the sintered pellet are then polished using fine emery paper on its (100) planes. Then these are coated with highly conducting pure silver paste which acts as electrodes to carry out further electrical characterization using a high-frequency LCR analyser (model PSM 1735-Numetri-Q phase-sensitive multimeter, N4L, Newtons4th Ltd., UK). Here the parallel plate method has been adopted for the permittivity measurement. Along with this, a laboratory fabricated pit furnace with a sample holding facility has been used in the designed experimental setup. To record the continuous experimental temperature a chromel–alumel thermocouple (type K) digital panel meter (Rishabh N25) has been used. A schematic diagram for the fabrication process corresponding to the experimental part is illustrated in Fig. 1.

3 Structural and Morphological Observations

Figure 2 depicts the XRD (x-ray diffraction) analysis of the calcined fine powder of PBNW sample at room temperature. The structural and lattice parameters have been identified

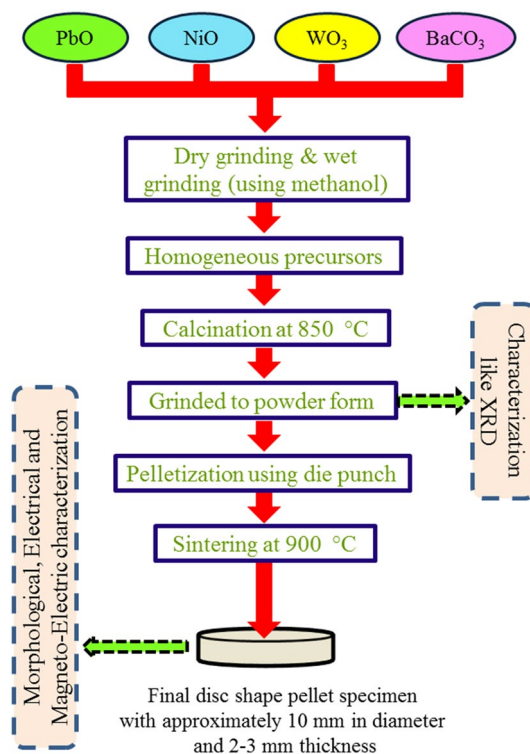


Fig. 1 Schematic diagram of fabrication processes

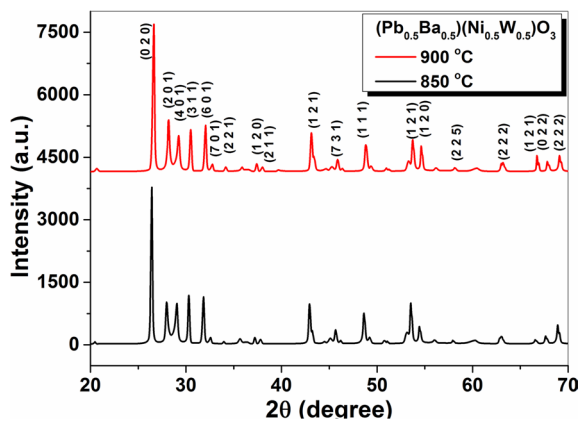


Fig. 2 Room temperature XRD pattern of $(\text{Pb}_{1/2}\text{Ba}_{1/2})(\text{Ni}_{1/2}\text{W}_{1/2})\text{O}_3$ calcined at 850 °C and 900 °C

from this pattern. By analyzing all the reflection peaks the formation of the new compound has been confirmed which is quite different from the original ingredients. All the major XRD peaks have been analyzed by using commercially available 'POWD' programming tools [17]. The structural portion of the compound has been investigated with a Bragg angle (2θ) and their intensity peaks in various crystal systems. Employing a worthy settlement among calculated value and the simulated value, the orthorhombic crystal system has been identified. The least-squares values lattice with proper refinement practice were found to be: $a = 6.3172 \text{ \AA}$, $b = 11.8041 \text{ \AA}$, $c = 7.8933 \text{ \AA}$ and $V = 588.59 \text{ \AA}^3$. The obtained normalized, unit cell dimension is considered as distorted perovskite.

Figure 3 shows the grayscale SEM images of the sintered PBNW pellet. From the SEM coagulated grains without having sharp boundaries are observed. A dense microstructure is observed which may be due to the melting behavior of the compound and it is visible in the image. This melting behavior may be due to the variations of melting points of different transition elements. Further from the EDAX analysis the presence of different elements along with their atomic percentage has been confirmed which is shown in Fig. 4. From this figure, it is also confirmed that the synthesized compound doesn't have any impurity in it. The elemental percentage obtained from both the calculated source and the EDAX source has been given in the Table 1.

4 Dielectric Study

To study the dielectric properties, relative permittivity (ϵ_r) versus temperature (T) as well as loss tangent ($\tan\delta$) versus temperature at typical selected frequencies (10 kHz, 25 kHz, 100 kHz, 500 kHz, and 1 MHz) over a temperature of (25–500 °C) are plotted for the synthesized sample PBNW

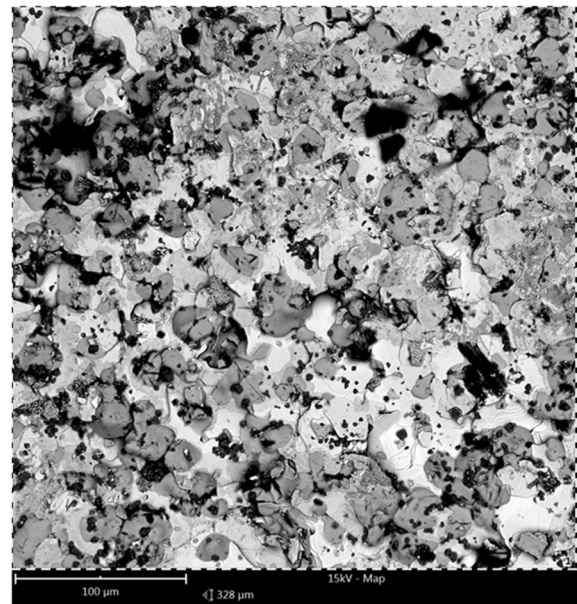


Fig. 3 Room temperature SEM micrograph of $(\text{Pb}_{1/2}\text{Ba}_{1/2})(\text{Ni}_{1/2}\text{W}_{1/2})\text{O}_3$

is depicted in Fig. 5a and b respectively. The dielectric constant has been calculated from the mathematical expression, $\epsilon_r = (C_p * d) / (\epsilon_0 * A)$, where ' C_p ' is the parallel capacitance, $A = \pi r^2$ (m^2) is the effective area, ' d ' is the thickness of the pellet sample, and $\epsilon_0 = 8.854 \times 10^{-12}$ (F/m) is the free space permittivity. From the dielectric plot Fig. 5a, it is observed that the rise in relative dielectric constant (ϵ_r) is very slow and almost frequency independent wherein at a temperature beyond 250 °C its value rises sharply with increasing slope and also frequency-dependent. With the rise in frequencies, the materials net polarization gradually ceases as the charge moment can't keep up with the alternating electric field, and hence the dielectric constant declines with higher frequencies. At high temperature, the rise in relative permittivity may be due to the heat and orientational polarization, creation of space charge polarization due to oxygen vacancies along with hopping of charge carriers during the sintering process [18]. A similar trend is also observed for the tangent loss vs temperature plot which is also given in Fig. 5b. The plot signifies dielectric absorption is more at higher temperatures. With an increase in temperature crystal structure becomes more and more distortive which results in the displacement of cations and the creation of dipolar moments. At low temperature due to dearth of thermally energized carriers, vacancies and imperfections the tangent loss decreases. These may enhance the hopping phenomena which result in higher tangent loss.

Frequency-dependent dielectric permittivity and tangent loss of synthesized PBNW at few selected temperature is depicted in Fig. 6a and b respectively. It has been

Fig. 4 Measured composition EDAX graphs of $(\text{Pb}_{1/2}\text{Ba}_{1/2})(\text{Ni}_{1/2}\text{W}_{1/2})\text{O}_3$

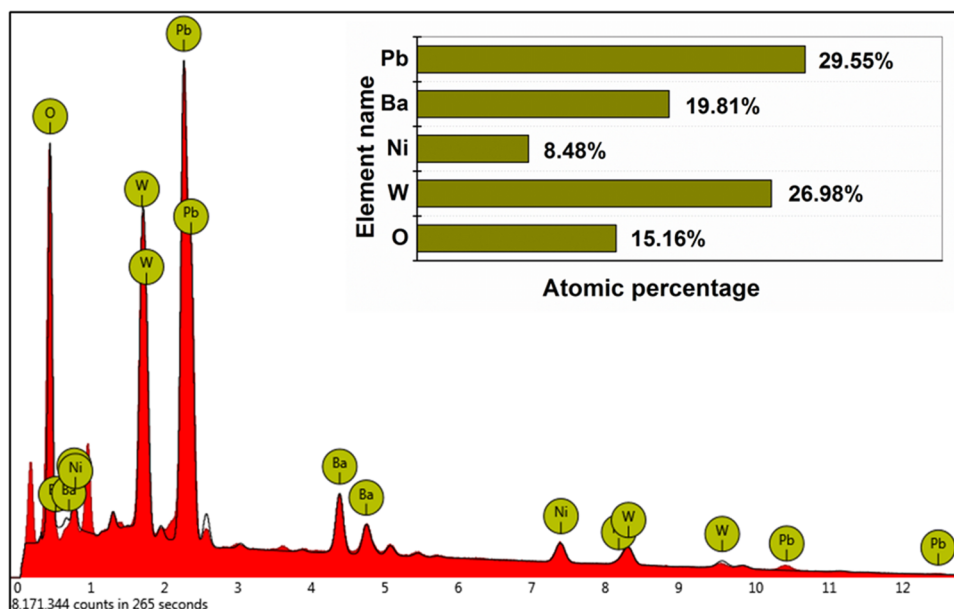


Table 1 Calculated and practical chemical content in the compound $(\text{Pb}_{1/2}\text{Ba}_{1/2})(\text{Ni}_{1/2}\text{W}_{1/2})\text{O}_3$

Element name	Cal. wt. (%)	Prac. wt. (%)	% of error
Pb	30.33	29.55	2.57
Ba	20.10	19.81	1.40
Ni	8.59	8.48	1.30
W	26.91	26.98	2.60
O	14.05	15.16	7.90

observed that the dielectric constant decreases with the rise in frequency. This is the usual characteristic of a dielectric. The rise in dielectric constant at low frequencies may be ascribed due to the existence of different polarizations like atomic, dipolar, ionic, and electronic polarization along with space charge accumulation at the electrode interface of the pellet. At the higher frequencies, the effect of polarization gradually diminished and the dielectric value merges. Also due to the relaxation process at high temperature as well as frequencies the dielectric permittivity merges. This is due to the decrease in interaction time for the polarization phenomena. A similar trend has been observed for tangent loss except for a peak at a high temperature. This peak appears may be due to the oscillation of the oxidation state through the transition metals, oxygen vacancies, and unknown defects [19]. The charges migrate within the impurity regions and store at interphases are trapped at grain boundaries. There appears field distribution due to build-up space charges and this shows an increase in permittivity known as interfacial polarization.

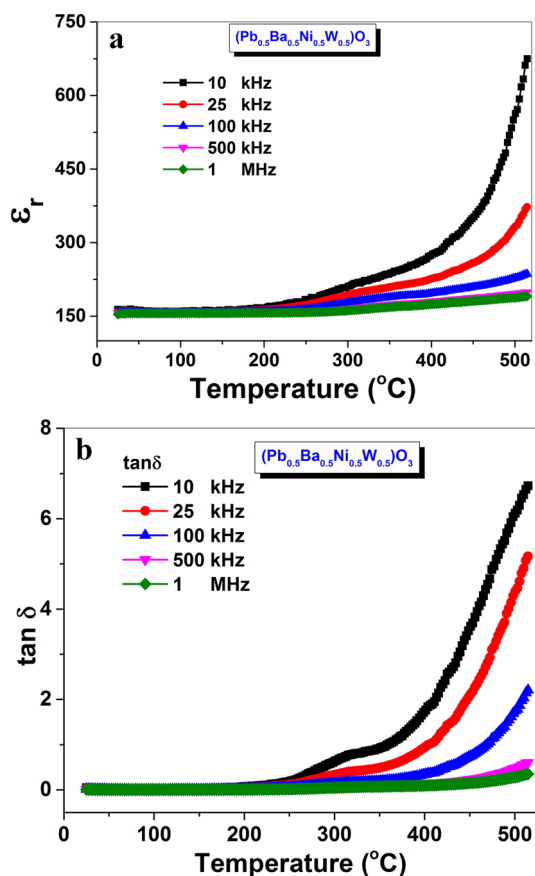


Fig. 5 Temperature dependence of **a** dielectric constant at selected frequencies of $(\text{Pb}_{1/2}\text{Ba}_{1/2})(\text{Ni}_{1/2}\text{W}_{1/2})\text{O}_3$, **b** tangent loss at selected frequencies of $(\text{Pb}_{1/2}\text{Ba}_{1/2})(\text{Ni}_{1/2}\text{W}_{1/2})\text{O}_3$

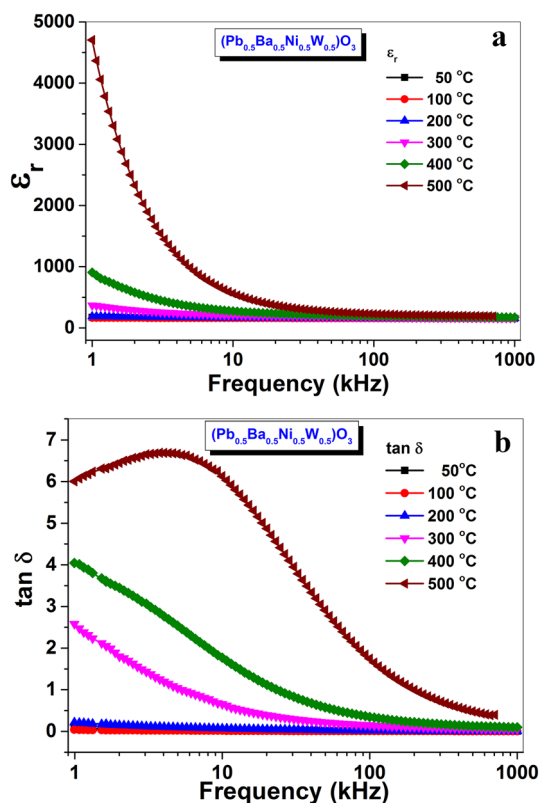


Fig. 6 Frequency dependence of **a** dielectric constant at specific temperatures of $(Pb_{1/2}Ba_{1/2})(Ni_{1/2}W_{1/2})O_3$, **b** tangent loss at specific temperatures of $(Pb_{1/2}Ba_{1/2})(Ni_{1/2}W_{1/2})O_3$

5 Conductivity Analysis

The frequency (1 kHz to 1 MHz) dependent electrical conductivity of the synthesized compound PBNW has been depicted in Fig. 7. The ac electrical conductivity of the

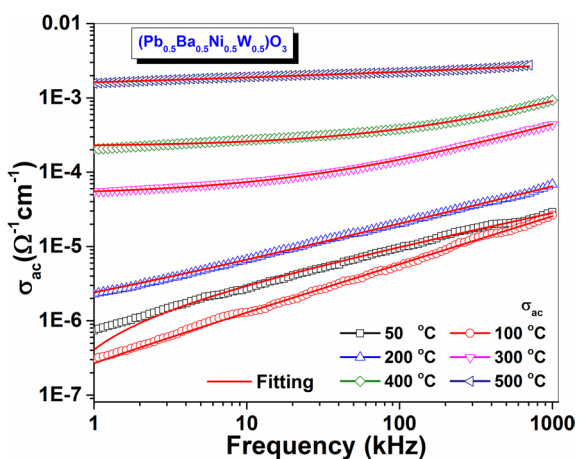


Fig. 7 Frequency dependent ac conductivity spectrum at selected temperature of $(Pb_{1/2}Ba_{1/2})(Ni_{1/2}W_{1/2})O_3$

fabricated sample has been evaluated by using the relation given as:

$$\sigma_{ac} = 2\pi f \epsilon_r \epsilon_0 \tan \delta \tag{1}$$

where f is the applied frequency, ϵ_r = relative dielectric constant, ϵ_0 = permittivity of free space, $\tan \delta$ = tangent loss.

From the figure, it can be concluded that at higher frequencies there is an increase in the ac conductivity and at lower frequencies the conductivity decreases. The increases in conductivity may be due to the contribution of polarons which are hopping around the smaller distances in the lattice. These polarons originated in the oxides due to the ionic creation/substitution of oxygen vacancies, disarranging of cations, and presence of multiple oxidation states of the transition elements. Again it is also observed that at higher frequencies the conductivities at different temperature moves closure/converge to each other whereas at lower frequencies they move apart. This sensation is known as low-frequency dispersion. This behavior is endorsed due to the interfacial polarization.

The frequency dependence conductivity is governed by the Jonscher’s power law [20, 21] which is:

$$\sigma_{ac} = \sigma_{dc} + A\omega^n \tag{2}$$

where σ_{ac} = ac conductivity, σ_{dc} = zero frequency conductivity, ω = angular frequency ($2\pi f$) and n = power-law exponent where its value lies between 0 and 1. This law can be used to estimate the conductivity through a wide frequency range. Analysis of high-frequency conductivity dispersion has been carried out by using Jonscher’s power law. The values of the fitting parameters A and n are given in the Table 2. The ac conductivity augmentation with the temperature of the synthesized compound at higher frequencies may be due to the diminution in barrier properties. From the table as the n value is less than 1, it suggests non-Debye type material.

The dependence of conductivity on inverse temperature has been illustrated in Fig. 8. Using the Arrhenius relation, the activation energy (E_a) for the thermally activated hopping process can be calculated. The activation energy value

Table 2 The values of σ_{dc} , A and n at different temperatures of the compound $(Pb_{1/2}Ba_{1/2})(Ni_{1/2}W_{1/2})O_3$

Temperature (°C)	σ_{dc}	A	n
50	-1.09×10^{-6}	7.60×10^{-8}	4.31×10^{-1}
100	-3.33×10^{-8}	3.54×10^{-9}	6.40×10^{-1}
200	5.00×10^{-7}	5.72×10^{-8}	5.08×10^{-1}
300	4.90×10^{-5}	9.64×10^{-8}	6.02×10^{-1}
400	2.22×10^{-4}	1.12×10^{-7}	6.31×10^{-1}
500	9.79×10^{-4}	2.35×10^{-4}	1.24×10^{-2}

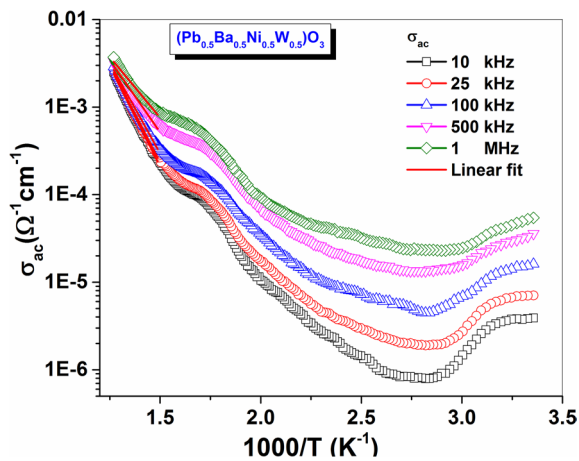


Fig. 8 Temperature dependent ac conductivity spectrum at selected frequency of $(\text{Pb}_{1/2}\text{Ba}_{1/2})(\text{Ni}_{1/2}\text{W}_{1/2})\text{O}_3$

Table 3 Activation energy at different frequencies of the compound $(\text{Pb}_{1/2}\text{Ba}_{1/2})(\text{Ni}_{1/2}\text{W}_{1/2})\text{O}_3$

Activation energy of PbBaNiWO_3 at the temperature range 400–500 °C		
1	10 kHz	0.91 eV
2	25 kHz	0.88 eV
3	100 kHz	0.82 eV
4	500 kHz	0.65 eV
5	1 MHz	0.55 eV

is obtained by fitting its dc conductivity by using the equation given as

$$\sigma_{ac} = \omega \epsilon \epsilon_0 \tan \delta \quad (3)$$

$$\sigma_{ac} = \sigma_0 \exp(-E_a/kT) \quad (4)$$

Here ϵ_0 , σ_0 and k take their usual meaning. The multiple linear fitting slopes signify the presence of multiple conduction phenomena which may arise due to the hopping phenomena of charge carriers at higher temperatures [22]. The multiple oxidation states of the transition metals help in this process. At high temperatures, the conductivity curve merges suggesting the frequency-independent properties of the material. The calculated activation energy from the slope is given in the Table 3. From these data, it is clear that activation energy is inversely proportional to frequency.

6 Nyquist Plot

The complex impedance analysis ie, the plot of Z'' (imaginary part of impedance) versus Z' (real part of impedance) at selected temperatures is illustrated in Fig. 9. This complex

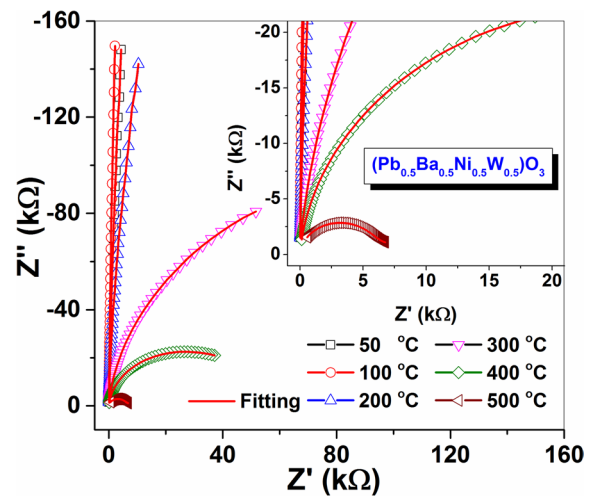


Fig. 9 Nyquist plot of $(\text{Pb}_{1/2}\text{Ba}_{1/2})(\text{Ni}_{1/2}\text{W}_{1/2})\text{O}_3$

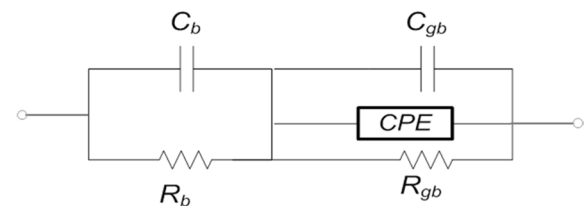


Fig. 10 Equivalent electrical circuit of the $(\text{Pb}_{1/2}\text{Ba}_{1/2})(\text{Ni}_{1/2}\text{W}_{1/2})\text{O}_3$ obtained using Z-win software

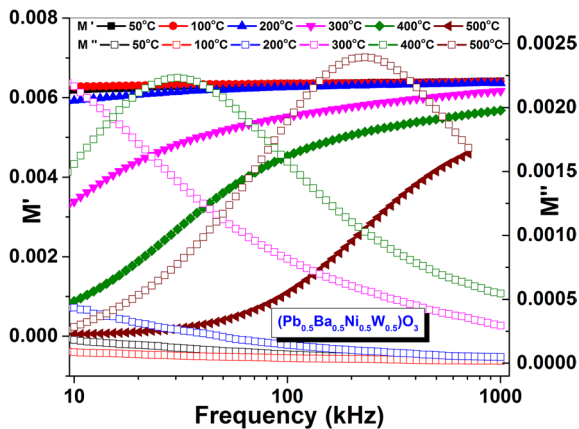
plot obtained over a wide range of temperature and frequency, predicts the grain, grain boundary, and electrode interface properties of the sample. It is observed that with ascend in temperature semicircle forming tendency increases (ie, the radius of the semicircle decreases). To study the equivalent circuit of this material as well as its grain, grain boundary, and electrode interface effect, these obtained data are compared with the fitted data which is obtained with the help of z-win software. The obtained equivalent circuit is given in the Fig. 10 and the values of C_b , R_b , R_{gb} , C_{gb} , and C_{PE} for different selected temperatures is given in the Table 4, where R_b = bulk resistance, C_b = bulk capacitance, C_{gb} = grain capacitance, R_{gb} = grain resistance, and C_{PE} = constant phase element respectively. The nonexistence of perfect semicircular arc suggests the non-Debye-type relaxation phenomena [23–26].

7 Complex Electric Modulus Analysis

The electrical relaxation and conduction phenomena of this compound can be analyzed extensively using the complex electrical modulus technique. The electric modulus

Table 4 Comparison of fitting parameters of bulk and grain boundary resistance as well as capacitance of impedance parameters of the compound $(\text{Pb}_{1/2}\text{Ba}_{1/2})(\text{Ni}_{1/2}\text{W}_{1/2})\text{O}_3$

Temperature (°C)	R_b (Ω)	C_b (F)	R_{gb} (Ω)	CPE	C_{gb}
50	6.82×10^4	1.53×10^{-7}	2.16×10^4	9.61×10^{-10}	3.92×10^{-5}
100	2.56×10^4	2.91×10^{-6}	4.05×10^4	5.02×10^{-8}	8.57×10^{-5}
200	3.74×10^3	1.42×10^{-6}	9.81×10^3	1.91×10^{-9}	7.98×10^{-4}
300	1.41×10^2	6.34×10^{-5}	3.48×10^5	7.06×10^{-8}	1.43×10^{-6}
400	8.37×10^2	8.20×10^{-5}	5.45×10^5	3.58×10^{-8}	1.27×10^{-6}
500	5.35×10^2	2.18×10^{-6}	8.75×10^5	3.25×10^{-6}	7.88×10^{-6}

**Fig. 11** Complex electrical modulus spectrum of $(\text{Pb}_{1/2}\text{Ba}_{1/2})(\text{Ni}_{1/2}\text{W}_{1/2})\text{O}_3$

characteristics of both M' (real component) and M'' (imaginary component) versus frequency at some selected temperatures of PBNW have been illustrated in Fig. 11. From the M' versus frequency plot it is observed that at higher frequencies the M' moves closer to each other. The presence of short-range mobility of the charge carriers and multiple conduction process is the cause of this kind of behavior. From the figure, it is marked that the imaginary part (M'') increases with the frequency and a maxima peak has been noticed which proves the existence temperature-dependent dielectric relaxation. Multiple peaks at different temperatures have been observed due to this relaxation process. Also, it can be noted that with the rise in frequency M'' increases and a maximum value/peak (M'' max) is obtained, which signifies the presence of temperature dependence of the dielectric relaxation. This relaxation phenomenon is the cause of multiple peaks observed in the plots. The peaks shift their position with the rise in temperature. At high temperature the hopping mechanism of charge carriers normally dominates. From the asymmetric peak broadening the presence of a non-Debye type of relaxation, behavior can be recommended, which indicates the dispersion of relaxation time with different time constants [27].

8 Conclusion

The compound PBNW has been formulated and synthesized using a solid-state reaction path. The prepared compound is found to be orthorhombic crystal structure from the room temperature x-ray diffraction analysis. Compact and melting like grains obtained from the SEM analysis with little or no void. Both frequency and temperature-dependent electrical parameters (Relative permittivity, loss tangent, conductivity, complex impedance, etc.) have been studied. The frequency dependent conductivity obeys the Joncher's power law which has been confirmed from the fitting parameters. From the conductivity analysis dominance of thermally activated process has been observed. From the IS analysis non-Debye type relaxation phenomena have been observed. These properties of this compound may be helpful for the development of new electronics devices.

In future work more novel double perovskite materials can be explored by doing more substitution of +2 oxidation state materials (such as Ca^{2+} , Sr^{2+} , Ba^{2+} , Ni^{2+} , Co^{2+} , Mn^{2+} , Ga^{2+} etc.) in 'A' site and +4 oxidation state materials (Ti^{4+} , Mn^{4+} , Ce^{4+} , Th^{4+} , etc.) in the 'B' site. +3 oxidation state metals can also be substituted on both the sites.

Declarations

Conflict of interests On behalf of all authors, the corresponding author states that there is no conflict of interest.

References

1. Z. Zhang, G. Yang, *J. Mater. Sci.: Mater. Electron.* **32**, 12758 (2021)
2. S.N. Das, *J. Appl. Phys.* **128**, 114101 (2020)
3. N. Jeon, J. Noh, W. Yang et al., *Nature* **517**, 476 (2015)
4. X. Tian, H. Dou, L. Wu, *J. Mater. Sci. Mater. Electron.* **31**, 3944 (2020)
5. S.N. Das, S.K. Pardhan et al., *J. Mater. Sci. Mater. Electron.* **29**, 9375 (2018)
6. G.R. Gajula, K.N. Chidambara Kumar, L.R. Buddiga et al., *J. Mater. Sci. Mater. Electron.* **30**, 3889 (2019)

7. A. Tripathy, S.N. Das, S. Bhuyan, R.N.P. Choudhary, *Trans. Electr. Electron. Mater.* **20**, 280 (2019)
8. K.G. Prasad, M.K. Niranjana, S. Asthana, *Physica B* **506**, 42 (2017)
9. W.S. Kim, E.S. Kim, K.H. Yoon, *J. Am. Ceram. Soc.* **82**, 2111 (1999)
10. V.L. Mathe, K.K. Patankar, R.N. Patil, C.D. Lokhande, *J. Mag. Mater.* **270**, 380 (2004)
11. M. Chickpatil, G.M. Chitgopikar, R.L. Raibagkar, *J. Mater. Sci. Mater. Electron.* **18**, 991 (2007)
12. M. Ghasdi, H. Alamdari, S. Royer, A. Adnot, *Sens. Actuators B* **156**, 147 (2011)
13. S. Okada et al., *Appl. Phys. Lett.* **108**, 251905 (2016)
14. H. Ding, A.V. Virkar, M. Liu, F. Lieu, *Phys. Chem. Chem. Phys.* **15**, 489–496 (2013)
15. H.J. Munoz, S.A. Korili, A. Gil, *Materials* **15**, 3288 (2022)
16. S.N. Das, S.K. Pardhan et al., *J. Electron. Mater.* **47**, 843 (2018)
17. E. Wu, *J. Appl. Cryst.* **22**, 506 (1989)
18. J. Cheng, S.W. Yu, J. Chen, Z. Meng, L.E. Cross, *Appl. Phys. Lett.* **89**, 122911 (2006)
19. T. Tsurumi, T. Harigai, in *Handbook of Advanced Dielectric, Piezoelectric and Ferroelectric Materials* (2008)
20. A.K. Jonscher, *Nature* **267**, 673 (1977)
21. S.N. Das, A. Pattanaik, S. Kadambini, S. Pradhan, S. Bhuyan, *J. Mater. Sci. Mater. Electron.* **27**, 10099 (2016)
22. A. Tripathy et al., *J. Mater. Sci. Mater. Electron.* **29**, 4770 (2018)
23. K.K. Mishra, A.T. Satya, A. Bharathi, V. Sivasubramanian, V.R.K. Murthy, A.K. Arora, *J. Appl. Phys.* **110**, 123529 (2011)
24. S.K. Pradhan, S.N. Das, S. Bhuyan, C. Behera, R. Padhee, R.N.P. Choudhary, *Appl. Phys. A* **122**, 604 (2016)
25. Y. Liu, J. Wei et al., *J. Mater. Sci. Mater. Electron.* **27**, 3095 (2016)
26. V. Provenzano, L.P. Boesch, V. Volterra, C.T. Moynihan, P.B. Macedo, *J. Am. Ceram. Soc.* **55**, 492 (1972)
27. R. Macdonald, *Solid State Ionics* **13**, 147 (1984)

Publisher's Note Springer Nature remains neutral with regard to jurisdictional claims in published maps and institutional affiliations.

Springer Nature or its licensor holds exclusive rights to this article under a publishing agreement with the author(s) or other rightsholder(s); author self-archiving of the accepted manuscript version of this article is solely governed by the terms of such publishing agreement and applicable law.